

# Ultrasonically Induced Sulfur-Doped Carbon Nitride/Cobalt Ferrite Nanocomposite for Efficient Sonocatalytic Removal of Organic Dyes

## Authors:

Surabhi Kamal, Guan-Ting Pan, Siewhui Chong, Thomas Chung-Kuang Yang

Date Submitted: 2020-02-12

Keywords: catalyst, cobalt ferrite, carbon nitride, ultrasound, organic dye, ultrasound-assisted degradation, sonocatalyst, nanocomposite, SCN/CoFe<sub>2</sub>O<sub>4</sub>

## Abstract:

The sulfur-doped carbon nitride/cobalt ferrite nanocomposite (SCN/CoFe<sub>2</sub>O<sub>4</sub>) was prepared via ultrasonication and studied for the sonocatalytic degradation of wastewater organic dye pollutants including methylene blue, rhodamine B, and Congo red. The X-ray photoelectron spectroscopy confirmed the presence and atomic ratios of S, C, N, Co, Fe, and O elements and their corresponding bonds with Co<sup>2+</sup> and Fe<sup>3+</sup> cations. The nanocomposite was found to have aggregated nanoparticles on a sheet-like structure. The bandgap energy was estimated to be 1.85 eV. For the sonocatalytic degradation of 25-ppm methylene blue at 20 kHz, 1 W and 50% amplitude, the best operating condition was determined to be 1 g/L of catalyst dosage and 4 vol % of hydrogen peroxide loading. Under this condition, the sonocatalytic removal efficiency was the highest at 96% within a reaction period of 20 min. SCN/CoFe<sub>2</sub>O<sub>4</sub> outperformed SCN and CoFe<sub>2</sub>O<sub>4</sub> by 2.2 and 6.8 times, respectively. The SCN/CoFe<sub>2</sub>O<sub>4</sub> nanocomposite was also found to have good reusability with a drop of only 7% after the fifth cycle. However, the degradation efficiencies were low when tested with rhodamine B and Congo red due to difference in dye sizes, structural compositions, and electric charges.

Record Type: Published Article

Submitted To: LAPSE (Living Archive for Process Systems Engineering)

Citation (overall record, always the latest version):

LAPSE:2020.0229

Citation (this specific file, latest version):

LAPSE:2020.0229-1

Citation (this specific file, this version):

LAPSE:2020.0229-1v1

DOI of Published Version: <https://doi.org/10.3390/pr8010104>

License: Creative Commons Attribution 4.0 International (CC BY 4.0)

Article

# Ultrasonically Induced Sulfur-Doped Carbon Nitride/Cobalt Ferrite Nanocomposite for Efficient Sonocatalytic Removal of Organic Dyes

Surabhi Kamal <sup>1</sup>, Guan-Ting Pan <sup>1</sup> , Siewhui Chong <sup>2</sup>  and Thomas Chung-Kuang Yang <sup>1,\*</sup> 

<sup>1</sup> Department of Chemical Engineering and Biotechnology, National Taipei University of Technology, No. 1, Section 3, Zhongxiao East Road, Da'an District, Taipei 106, Taiwan; surabhi.chem30@gmail.com (S.K.); gtpan@ntut.edu.tw (G.-T.P.)

<sup>2</sup> Department of Chemical and Environmental Engineering, University of Nottingham Malaysia, Broga Road, Semenyih, Selangor 43500, Malaysia; faye.chong@nottingham.edu.my

\* Correspondence: ckyang@mail.ntut.edu.tw

Received: 21 November 2019; Accepted: 3 January 2020; Published: 13 January 2020



**Abstract:** The sulfur-doped carbon nitride/cobalt ferrite nanocomposite (SCN/CoFe<sub>2</sub>O<sub>4</sub>) was prepared via ultrasonication and studied for the sonocatalytic degradation of wastewater organic dye pollutants including methylene blue, rhodamine B, and Congo red. The X-ray photoelectron spectroscopy confirmed the presence and atomic ratios of S, C, N, Co, Fe, and O elements and their corresponding bonds with Co<sup>2+</sup> and Fe<sup>3+</sup> cations. The nanocomposite was found to have aggregated nanoparticles on a sheet-like structure. The bandgap energy was estimated to be 1.85 eV. For the sonocatalytic degradation of 25-ppm methylene blue at 20 kHz, 1 W and 50% amplitude, the best operating condition was determined to be 1 g/L of catalyst dosage and 4 vol % of hydrogen peroxide loading. Under this condition, the sonocatalytic removal efficiency was the highest at 96% within a reaction period of 20 min. SCN/CoFe<sub>2</sub>O<sub>4</sub> outperformed SCN and CoFe<sub>2</sub>O<sub>4</sub> by 2.2 and 6.8 times, respectively. The SCN/CoFe<sub>2</sub>O<sub>4</sub> nanocomposite was also found to have good reusability with a drop of only 7% after the fifth cycle. However, the degradation efficiencies were low when tested with rhodamine B and Congo red due to difference in dye sizes, structural compositions, and electric charges.

**Keywords:** SCN/CoFe<sub>2</sub>O<sub>4</sub>; nanocomposite; sonocatalyst; ultrasound-assisted degradation; organic dye; ultrasound; carbon nitride; cobalt ferrite; catalyst

## 1. Introduction

The risk of environmental pollution has increased rapidly due to the industrial and economic development. Industries such as paper mills, pharmaceutical, textile, dyeing, and cosmetics using a huge amount of organic dyes result in the production of persistent pollutants that are difficult to degrade after discharge, which further leads to the emergence of secondary pollutants [1,2]. Various techniques have been proposed for the removal of water-soluble pollutants such as adsorption, sedimentation, chemical precipitation, membrane technologies, electrochemical and oxidation processes [3–5].

Recently, great attention has been given to sonodegradation as an advanced oxidation process (AOP) for wastewater treatments. The abrupt growth, as well as the collapse of bubbles in solution under the ultrasound irradiation during the process, leads to extreme pressure and temperature around the bubbles [6,7]. The generation of a potent oxidizing agent like hydroxyl radicals (OH<sup>·</sup>) increases because of the high temperature around the bubbles, which is useful for the non-selective oxidation of organic dyes. Nonetheless, ultrasound waves alone are not sufficient for the degradation of organic pollutants due to the requirement of higher energy and time. Sonocatalyst is used to overcome this problem for degrading pollutants in the solution. Several nanomaterials, for example, Fe<sub>3</sub>O<sub>4</sub>, Cu:

ZnS-NPs-AC, TiO<sub>2</sub>, MgO ZnO, ZnS, Cu<sub>2</sub>S, CdS, MIL-101(Cr)/RGO/ZnFe<sub>2</sub>O<sub>4</sub> and CoFe<sub>2</sub>O<sub>4</sub>@ZnS have been used for sonocatalytic degradation of organic dyes [8–22].

Compared to the other catalyst materials, graphitic carbon nitride (g-C<sub>3</sub>N<sub>4</sub>) has been broadly studied for its appealing lamellar structure, low-cost, non-toxic, high abundance, and recyclability. Because of its fast electron-hole recombination rate and relatively low specific surface area, g-C<sub>3</sub>N<sub>4</sub> is doped with metals or non-metal species such as Fe, Ag, Au, O, B, and P, coupling with TaON, Bi<sub>2</sub>WO<sub>6</sub> [11,19,23–28]. Sulfur doped g-C<sub>3</sub>N<sub>4</sub> (SCN) effectively narrows down the bandgap with the enhancement of the catalytic activity. The electronegativity of S is lower than that of N, which results in its unique electronic structure where the S-doped levels are located above the maximum valence band of doped g-C<sub>3</sub>N<sub>4</sub>. However until now, little attention has been focused on SCN to investigate the sonocatalytic degradation of organic dyes [26,28].

The spinel ferrites having a general formula of MFe<sub>2</sub>O<sub>4</sub> (M = Mg, Ca, Mn, Co, Cu, Ni, Zn) are a close-packed array of O<sup>2-</sup> ions, with M<sup>2+</sup> and Fe<sup>3+</sup> cations located either partially or all of the tetrahedral and octahedral sites [8,29–36]. Among all ferrites, CoFe<sub>2</sub>O<sub>4</sub> (CFO) possessing the characteristic of an excellent magnetic, electrical property and chemical stability with abundance, low-cost, and eco-friendliness has significantly attracted attention for various purposes such as catalysis, batteries, environment remediation, hydrogen production, etc. [29,30,36].

In the present work, SCN/CoFe<sub>2</sub>O<sub>4</sub> nanocomposite was synthesized for the first time via the ultrasonication method. The sonocatalytic performance of SCN/CoFe<sub>2</sub>O<sub>4</sub> nanocomposite for degrading the organic wastewater dye pollutants including methylene blue (MB), rhodamine B (RhB), and Congo red (CR) was evaluated. The changes in the degradation efficiency for the important parameters including H<sub>2</sub>O<sub>2</sub> loading and catalyst dosage were also investigated. In addition, the sonocatalytic activities of pure SCN and CoFe<sub>2</sub>O<sub>4</sub> were carried out under the same conditions for a comparative study.

## 2. Materials and Methods

### 2.1. Materials

All chemicals—iron nitrate (Fe(NO<sub>3</sub>)<sub>3</sub>·9H<sub>2</sub>O, 99%, Grand Chemical Co., Ltd., Miaoli, Taiwan), cobalt nitrate (Co(NO<sub>3</sub>)<sub>2</sub>·6H<sub>2</sub>O, 99%, Merck, Taipei, Taiwan), dicyandiamide (C<sub>2</sub>H<sub>4</sub>N<sub>4</sub>, 99%, Grand Chemical Co., Ltd., Miaoli, Taiwan), sulfuric acid (H<sub>2</sub>SO<sub>4</sub>, Thermo Fisher Scientific, Taipei, Taiwan), hydrogen peroxide (30%, Merck, Taipei, Taiwan), and sodium hydroxide (NaOH, Nihon Shiyaku Industries Ltd., Taipei, Taiwan), were of analytical grade and used as received. Double-distilled water was used throughout the experiment.

### 2.2. Synthesis of SCN

In the simple synthesis of SCN, 5 g of dicyandiamide was mixed with dilute H<sub>2</sub>SO<sub>4</sub> [24]. This homogenous solution was heated at 100 °C under vigorous stirring to remove the water molecules. Further, the mixture was heated using a muffle furnace at 550 °C with a rate of 5 °C min<sup>-1</sup> for 3 h. Finally, the powder was collected after centrifugation, washed with ethanol/water and followed by drying in an oven for 4 h at 80 °C.

### 2.3. Ultrasonic Synthesis of SCN/CoFe<sub>2</sub>O<sub>4</sub> Nanocomposite

For synthesizing the SCN/CoFe<sub>2</sub>O<sub>4</sub> nanocomposite, 0.5 g of SCN was taken in 50 mL water and stirred for 15 min. To the above solution, 50 mL of Co(NO<sub>3</sub>)<sub>2</sub>·6H<sub>2</sub>O (1M) and 50 mL of Fe(NO<sub>3</sub>)<sub>3</sub>·9H<sub>2</sub>O (2M) were added and mixed using ultrasonication (Qsonica sonicators, Newtown borough, CT, USA) for 30 min at 20 kHz, 50% amplitude, and 1 W. The solution was maintained at pH ~ 11 by the addition of 1 M NaOH [29]. Further, the suspension was shifted into a 100 mL Teflon-lined stainless steel and autoclaved at 180 °C for 16 h. The as-formed sample was centrifuged, washed with ethanol/water, and kept for drying in the oven at 90 °C. The collected sample was labeled as SCN/CoFe<sub>2</sub>O<sub>4</sub>. A similar method was used for the synthesis of the CoFe<sub>2</sub>O<sub>4</sub> without the addition of SCN.

### 2.3.1. Characterization

The crystallinity and structural patterns of the samples were investigated by the X-ray diffractometer (XRD, PANalytical X'Pert PRO, Almelo, The Netherlands) with CuK  $\alpha$  radiation ( $\lambda = 1.5418$  Å). The structural studies of the samples were recorded using a field-emission scanning electron microscope (FESEM, JEOL JSM-7100F, Peabody, MA, USA) and a transmission electron microscopy (TEM, JEM2100F, Akishima, Japan) with 200 kV acceleration voltage. Fourier transform infrared (FT-IR, Perkin Elmer Spectrum GX, Shelton, WA, USA) was used to study the sample's structure. The FT-IR sample pellets were prepared using the KBr substrate. Cary 5000 UV-Vis-NIR spectrophotometer (Agilent, Santa Clara, CA, USA) with an integrating sphere attachment was used for UV-visible diffuse reflectance spectra (UV-DRS). Photoluminescence (PL) spectroscopy (Dongwoo-Ramboss 500i, Gyeonggi-do, Korea) was used to confirm the optical properties of synthesized materials and to calculate the lifetime of the excited electron (recombination rate). X-ray photoelectron spectroscopy (XPS, JEOL JPS-9030, Tokyo, Japan) was used to study the elemental composition and configuration of the samples.

### 2.3.2. Sonocatalytic Degradation of Organic Dyes

Organic dye removal in aqueous solutions was analyzed in the presence of SCN/CoFe<sub>2</sub>O<sub>4</sub> nanocomposite using the ultrasonication method at 20 kHz, 1 W, 50% amplitude, and pulse every 2 s [31]. The removal efficiencies of the catalysts CoFe<sub>2</sub>O<sub>4</sub> and SCN were also evaluated for benchmarking. Catalyst (50 mg) was added to 50 mL of a solution containing 25 ppm MB dye with 2 mL H<sub>2</sub>O<sub>2</sub> (i.e., catalyst dosage of 1 g/L and H<sub>2</sub>O<sub>2</sub> loading of 4 vol %). To balance the adsorption-desorption process between the catalyst and dye, the suspension was stirred magnetically without irradiation for 30 min. The experiment was then subjected to ultrasonic irradiation. Sample solution (2 mL) was taken at particular time intervals for monitoring the residual dye concentration using the UV-Vis spectrophotometer. The degradation efficiency (R) was calculated using Equation (1) and pseudo-first-order kinetic Equation (2) was used to evaluate the kinetic rate.

$$R\% = [(C_0 - C_t)/C_0] \times 100 \quad (1)$$

$$\ln(C_0/C) = kt \quad (2)$$

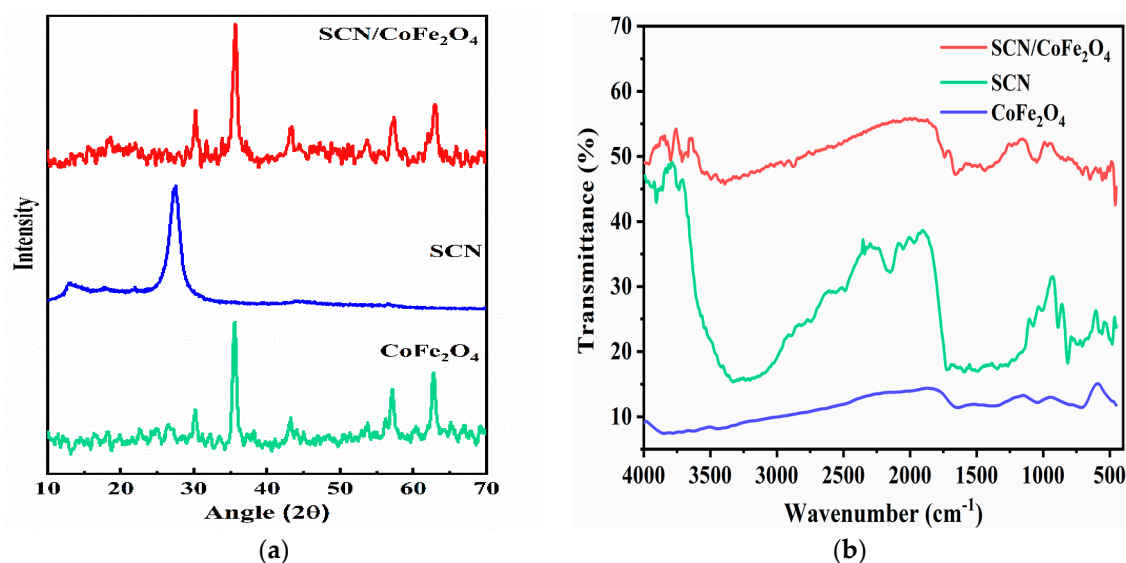
where  $C_0$  and  $C_t$  are the dye concentration before irradiation and after time  $t$  irradiation, respectively,  $C$  is the dye concentration,  $k$  is the rate constant, and  $t$  is the reaction time. The effects of the dosage of catalyst (0–1.5 g/L) and H<sub>2</sub>O<sub>2</sub> concentration (0–6 vol %) on the catalytic activity were also studied. For further examination of the effectiveness of the sonocatalyst, degradations of RhB and CR were also evaluated at similar conditions.

## 3. Results and Discussion

### 3.1. Characterizations of the SCN, CoFe<sub>2</sub>O<sub>4</sub> and SCN/CoFe<sub>2</sub>O<sub>4</sub> Catalysts

To investigate the structures and compositions of SCN, CoFe<sub>2</sub>O<sub>4</sub>, and SCN/CoFe<sub>2</sub>O<sub>4</sub>, XRD patterns were recorded. As shown in Figure 1a, the diffraction peaks for spinel CoFe<sub>2</sub>O<sub>4</sub> appear at  $2\theta = 30.16^\circ, 35.60^\circ, 38.21^\circ, 43.21^\circ, 53.64^\circ, 57.12^\circ, \text{ and } 62.77^\circ$ , indexed as (220), (311), (222), (400), (422), (511), and (440) planes respectively (JCPDS card No. 00-022-1086) [7,37,38]. SCN depicts the two characteristic diffraction peaks at  $27.42^\circ$  and  $13.04^\circ$  indexed as (002) and (100) planes (JCPDS card No. 87-1526) for SCN [24]. The peak around (002) corresponds to the lamellar stacking of the conjugated aromatic system and (100) for the in-plane packing of g-C<sub>3</sub>N<sub>4</sub>. The peaks for SCN/CoFe<sub>2</sub>O<sub>4</sub> composite occur at  $30.28^\circ, 35.60^\circ, 38.21^\circ, 43.21^\circ, 53.64^\circ, 57.12^\circ, \text{ and } 62.77^\circ$  which correspond to the (220), (311), (222), (400), (422), (511), and (440) planes respectively. The disappearance of the characteristic peaks of SCN in the SCN/CoFe<sub>2</sub>O<sub>4</sub> nanocomposite could be due to the anchoring of CoFe<sub>2</sub>O<sub>4</sub> nanoparticles on

the SCN sheets, which has prevented the SCN sheets from restacking orderly due to its small content in the nanocomposite [39].



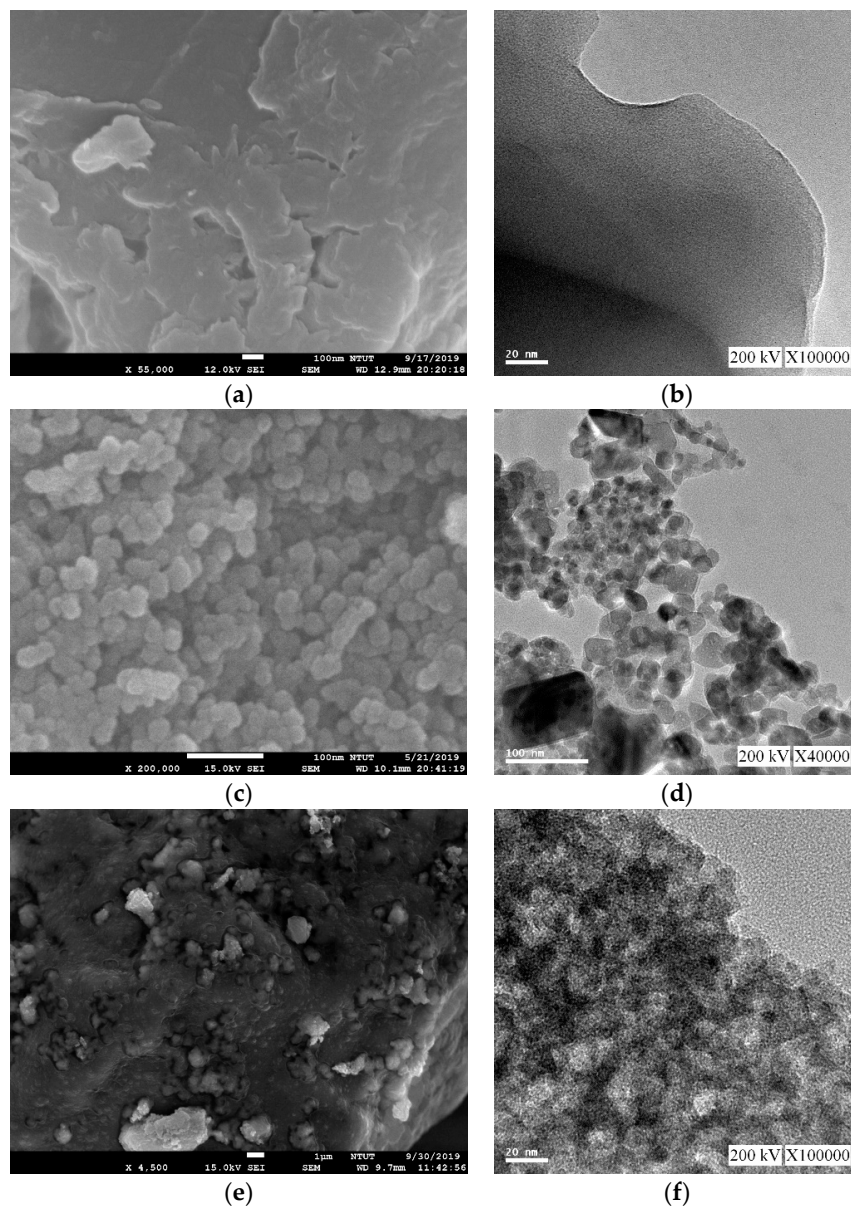
**Figure 1.** (a) XRD patterns of CoFe<sub>2</sub>O<sub>4</sub>, SCN, and SCN/CoFe<sub>2</sub>O<sub>4</sub> nanocomposite; (b) FT-IR spectra of CoFe<sub>2</sub>O<sub>4</sub>, SCN, and SCN/CoFe<sub>2</sub>O<sub>4</sub> nanocomposite.

Figure 1b displays the FT-IR spectra of the as-synthesized catalysts. For SCN, a broad stretching vibration peak of N-H or O-H group appears at 3100–3500 cm<sup>-1</sup>. The peaks for SCN at 810 and 890 cm<sup>-1</sup> are among the characteristic peaks of the CN condensed heterocycles and N-H vibrations, respectively. The bands from the 1237–1640 cm<sup>-1</sup> correspond to the typical heptazine ring units of g-C<sub>3</sub>N<sub>4</sub> [25]. Due to the small amount of sulfur doping, the vibrations of S-containing groups are absent. In CoFe<sub>2</sub>O<sub>4</sub> nanoparticles, the principal peak within the range of 400–600 cm<sup>-1</sup> is attributed to the Co-O and Fe-O bonds of spinel oxide [29]. Despite of the presence of a small amount of SCN, the peaks as seen in the SCN/CoFe<sub>2</sub>O<sub>4</sub> nanocomposite confirm the presence of CoFe<sub>2</sub>O<sub>4</sub> and SCN. These collectively proved the formation of SCN/CoFe<sub>2</sub>O<sub>4</sub> nanocomposite.

The size and morphology of CoFe<sub>2</sub>O<sub>4</sub>, SCN, and SCN/CoFe<sub>2</sub>O<sub>4</sub> nanocomposite were analyzed by FE-SEM and TEM as depicted in Figure 2. SCN possesses an irregular sheet-like structure based on Figure 2a,b [40–42]. As shown in Figure 2c,d, CoFe<sub>2</sub>O<sub>4</sub> exhibits irregular aggregates with particles ranging from 10.5 to 53 nm due to their strong magnetic properties and the dipole-dipole interactions between the magnetic aggregates [38,43,44]. Figure 2e,f shows that the SCN/CoFe<sub>2</sub>O<sub>4</sub> nanocomposite consists of aggregated nanoparticles embedded in the sheet-like SCN.

The UV-Vis absorption spectra measured in the wavelength range of 200 to 800 nm for the as-synthesized samples are displayed in Figure 3a. In comparison with the absorption spectra of SCN and CoFe<sub>2</sub>O<sub>4</sub>, SCN/CoFe<sub>2</sub>O<sub>4</sub> nanocomposite displayed an enhanced absorption capability with higher absorption intensity. Furthermore, the bandgap energies of the samples calculated from the plot of  $(\alpha h\nu)^2$  versus bandgap energy are presented in Figure 3b. The estimated bandgaps were 2.47, 1.37, and 1.85 eV for SCN, CoFe<sub>2</sub>O<sub>4</sub>, SCN/CoFe<sub>2</sub>O<sub>4</sub> nanocomposite, respectively. The reduction in the bandgap of SCN/CoFe<sub>2</sub>O<sub>4</sub> nanocomposite when compared with SCN is thus due to the presence of CoFe<sub>2</sub>O<sub>4</sub>.

The photoluminescence spectra of SCN, CoFe<sub>2</sub>O<sub>4</sub>, and SCN/CoFe<sub>2</sub>O<sub>4</sub> nanocomposite were analyzed to understand the recombination process of sonogenerated electrons and holes (e<sup>-</sup>-h<sup>+</sup>). In Figure 4 (inset), the SCN/CoFe<sub>2</sub>O<sub>4</sub> nanocomposite is shown to have the lowest PL intensity when compared to SCN and CoFe<sub>2</sub>O<sub>4</sub>, which infers to a higher ability to capture the sonogenerated electrons. Hence, SCN/CoFe<sub>2</sub>O<sub>4</sub> nanocomposite can efficiently lower the recombination rate of the sonogenerated charge carriers.



**Figure 2.** FESEM (a) and TEM (b) of SCN; FESEM (c) and TEM (d) of  $\text{CoFe}_2\text{O}_4$ ; FESEM (e) and TEM (f) of  $\text{SCN}/\text{CoFe}_2\text{O}_4$ .

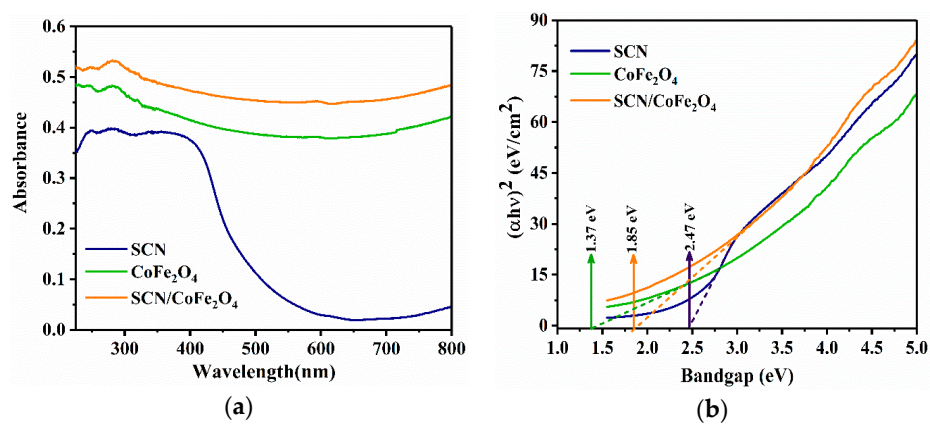


**Figure 3.** (a) UV-Vis spectra of SCN,  $\text{CoFe}_2\text{O}_4$ , and  $\text{SCN}/\text{CoFe}_2\text{O}_4$  nanocomposite; (b)  $(\alpha h\nu)^2$  vs. bandgap energy.

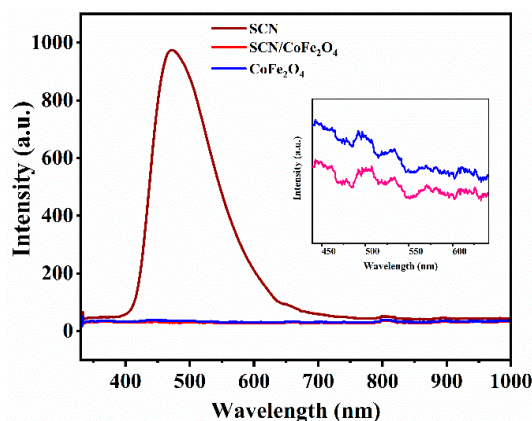


**Figure 4.** Photoluminescence spectra of SCN, CoFe<sub>2</sub>O<sub>4</sub> and SCN/CoFe<sub>2</sub>O<sub>4</sub> nanocomposite.

Figure 5 shows the XPS results of the samples. Figure 5a displays the C 1s spectrum where the four fitting peaks at 284.7, 285.9, 288.5, and 283.3 eV correspond to the C=C, N-C=N, C-C, and C-N/C-S bonds, respectively [25,28,45–49]. In Figure 5b, the three deconvoluted peaks for N 1s spectrum centered at 397.6, 399.8, 401.4, and 403.1 eV correspond to pyridinic N, tertiary nitrogen N-(C)<sub>3</sub>, N(C-H) group, and  $\pi$ -excitation [24–29]. The characteristic peaks of S 2p<sub>3/2</sub> at 162.7 and 168.4 eV, as seen in Figure 5c, arose from the C-S bond in SCN and S-O bond due to the surface adsorption of oxygen during the calcination process [27,28,30]. The Co 2p spectrum, depicted in Figure 5d, was attributed to the presence of Co<sup>2+</sup> cations. As seen, two characteristic peaks of Co 2p<sub>3/2</sub> at around 779.2 and 781.5 eV were due to the Co<sup>2+</sup> in B-sites and Co<sup>2+</sup> in A-sites with the corresponding shake-up satellite peaks at 784.9 and 789.7 eV [30–33]. Similarly, the Fe 2p<sub>3/2</sub> spectrum shown in Figure 5e is composed of two characteristic peaks at 709.4 and 710.8 eV, assigned to Fe<sup>3+</sup> at B-sites and Fe<sup>3+</sup> at A-sites along with shake-up satellites at 714.8 and 717.7 eV respectively [50–55]. Moreover, fitting peaks of O 1s reveal peaks at 529.6 and 530.8 eV, which coincide with the lattice oxygen and chemisorbed oxygen species, respectively, as displayed in Figure 5f [46,54]. XPS analysis also reveals the atomic ratios of C, Co, Fe, O, N, and S of the SCN/CoFe<sub>2</sub>O<sub>4</sub> nanocomposite to be 54.39%, 2.03%, 39.83%, 2.36%, and 0.94%, respectively.

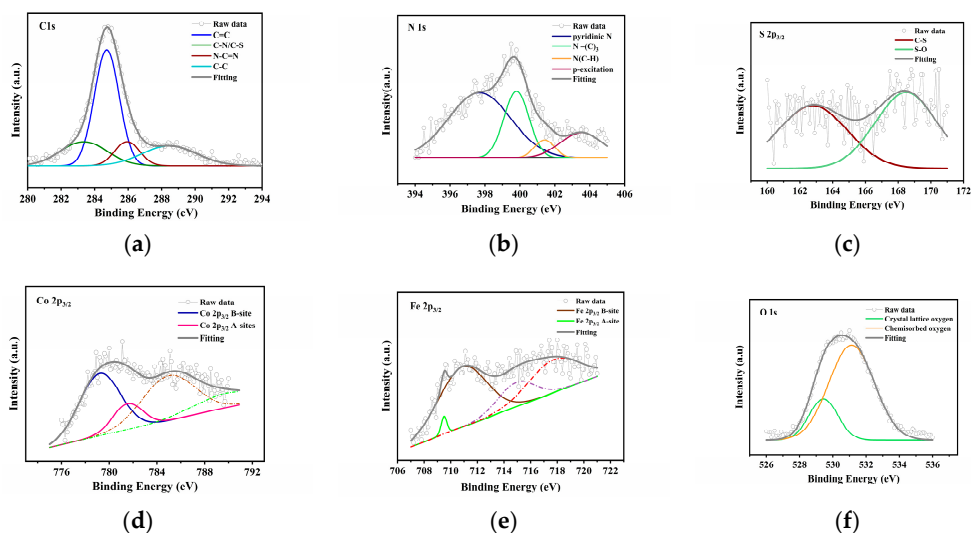


**Figure 5.** The XPS spectra of (a) C 1s; (b) N 1s; (c) S 2p; (d) Co 2p; (e) Fe 2p; (f) O 1s.

### 3.2. Effect of Catalyst Dosage

In order to study the catalyst dosage influence on the degradation of MB dye, the amount of SCN/CoFe<sub>2</sub>O<sub>4</sub> nanocomposite was varied from 0 to 1.5 g/L at H<sub>2</sub>O<sub>2</sub> loading of 4 vol % and without

ultrasonication. As shown in Figure 6, the degradation efficiency was very low in the absence of the catalyst at about 35% in 20 min. The increase in catalyst dosage from 0 to 0.5 g/L led to an increase in the degradation efficiency by 26%. This suggests that the higher amount of dosage favors the MB degradation due to the excess availability of the active sites which help in the generation of surplus hydroxyl radicals ( $\text{OH}\cdot$ ) for the degradation of MB [7]. However, as indicated by the drop in the degradation efficiency from 63 to 55% at the catalyst dosage of 1 and 1.5 g/L, respectively, an excess amount of catalyst dosage (in excess of 1 g/L) tends to decrease the selectivity and yield of  $\text{H}_2\text{O}_2$  to form undesired water [56].

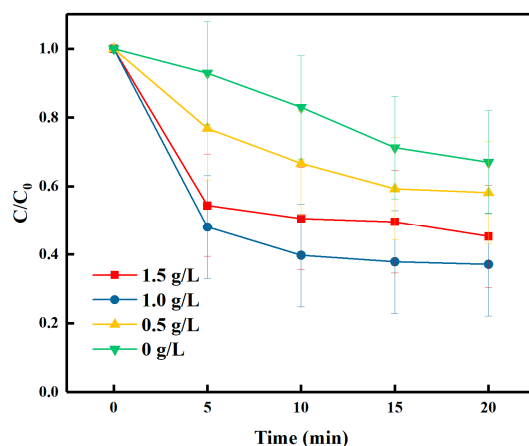


**Figure 6.** Effect of  $\text{SCN}/\text{CoFe}_2\text{O}_4$  dosage on the catalytic degradation of MB without ultrasonication. Experimental conditions:  $[\text{MB}] = 25 \text{ ppm}$ ,  $[\text{catalyst}] = 0\text{--}1.5 \text{ g/L}$ ,  $[\text{H}_2\text{O}_2] = 4 \text{ vol } \%$ .

### 3.3. Effect of $\text{H}_2\text{O}_2$ Loading

The influence of the amount of  $\text{H}_2\text{O}_2$  on the degradation of MB was investigated. As seen in Figure 7, only 14% of MB dye was degraded in the absence of  $\text{H}_2\text{O}_2$  within the reaction time of 20 min. The degradation efficiency was increased from 45% to 66% when the  $\text{H}_2\text{O}_2$  loading was increased from 2 and 4 vol % of  $\text{H}_2\text{O}_2$  due to the excess of  $\text{OH}\cdot$  with a higher amount of  $\text{H}_2\text{O}_2$ . However, an increase in the amount of  $\text{H}_2\text{O}_2$  from 4 to 6 vol % decreased the degradation efficiency to 57%. This is because surplus  $\text{H}_2\text{O}_2$  serves as a scavenger of hydroxyl radical to lower the oxidation potential by the generation of perhydroxyl radical ( $\text{HOO}\cdot$ ) [7,10,42].

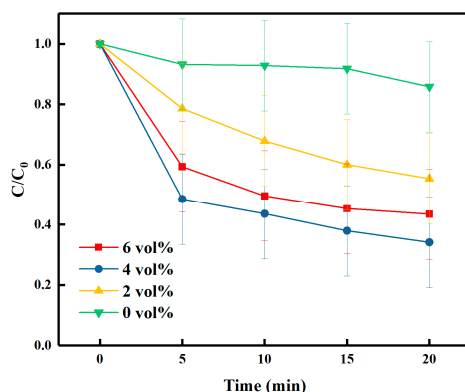


**Figure 7.** Effect of  $\text{H}_2\text{O}_2$  loading on the catalytic degradation of MB without ultrasonication. Experimental conditions:  $[\text{MB}] = 25 \text{ ppm}$ ,  $[\text{catalyst}] = 1 \text{ g/L mg}$ ,  $[\text{H}_2\text{O}_2] = 0\text{--}6 \text{ vol } \%$ .

### 3.4. Sonocatalytic Degradation Performances of the $\text{SCN}$ , $\text{CoFe}_2\text{O}_4$ and $\text{SCN}/\text{CoFe}_2\text{O}_4$ Catalysts

Using the best conditions obtained above—catalyst loading of 1 g/L and  $\text{H}_2\text{O}_2$  loading of 4 vol %—the catalytic and sonocatalytic degradations of 25-ppm methylene blue by  $\text{SCN}$ ,  $\text{CoFe}_2\text{O}_4$ ,



and SCN/CoFe<sub>2</sub>O<sub>4</sub> with and without the presence of H<sub>2</sub>O<sub>2</sub> and/or ultrasonication (US) were evaluated and the results are shown in Figure 8. Figure 8a displays a correlative study on the degradation of MB with US alone, H<sub>2</sub>O<sub>2</sub>/US, SCN/H<sub>2</sub>O<sub>2</sub>/US, CoFe<sub>2</sub>O<sub>4</sub>/H<sub>2</sub>O<sub>2</sub>/US, SCN/CoFe<sub>2</sub>O<sub>4</sub>/US, SCN/CoFe<sub>2</sub>O<sub>4</sub>/H<sub>2</sub>O<sub>2</sub>/US systems. The MB degradation efficiencies are in the following order: SCN/CoFe<sub>2</sub>O<sub>4</sub>/H<sub>2</sub>O<sub>2</sub>/US (96%) > H<sub>2</sub>O<sub>2</sub>/US (45%) > CoFe<sub>2</sub>O<sub>4</sub>/H<sub>2</sub>O<sub>2</sub>/US (43%) > SCN/CoFe<sub>2</sub>O<sub>4</sub>/H<sub>2</sub>O<sub>2</sub> (37%) > SCN/CoFe<sub>2</sub>O<sub>4</sub> (33%) > SCN/CoFe<sub>2</sub>O<sub>4</sub>/US (27%) > SCN/H<sub>2</sub>O<sub>2</sub>/US (14%) > US alone (11%).

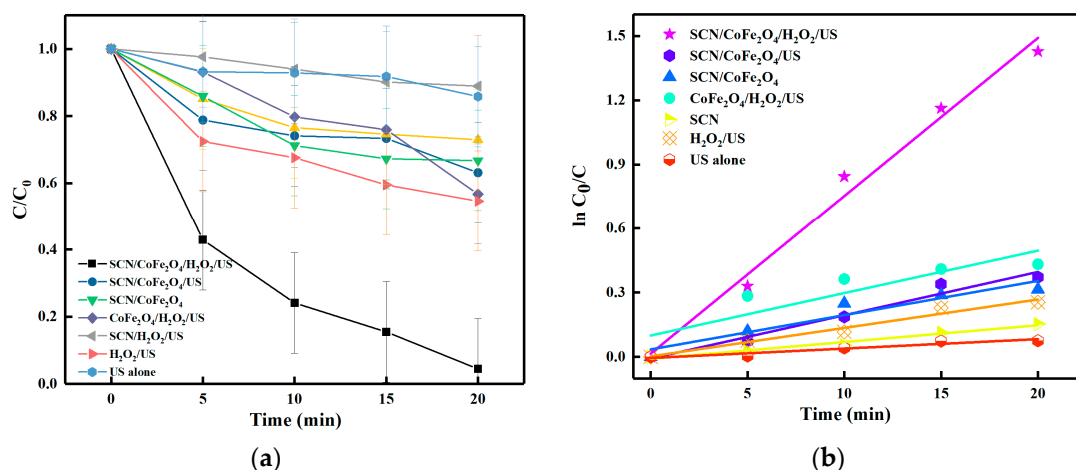


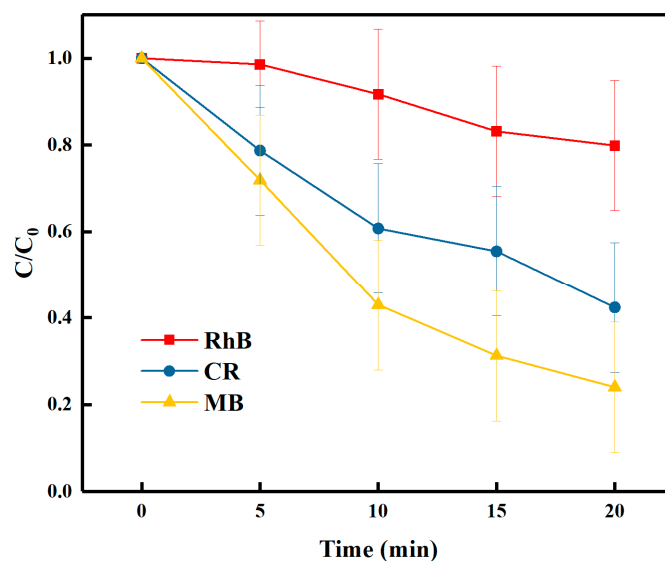
**Figure 8.** (a) Change in concentration of MB as a function of ultrasonication time; (b)  $\ln(C_0/C)$  versus ultrasonication time. Experimental conditions: [MB] = 25 ppm, [sonocatalyst] = 1 g/L, [H<sub>2</sub>O<sub>2</sub>] = 4 vol %.

The SCN/CoFe<sub>2</sub>O<sub>4</sub>/H<sub>2</sub>O<sub>2</sub>/US system exhibited the highest degradation activity of 96% in 20 min. By comparing the graphs of US alone with H<sub>2</sub>O<sub>2</sub>/US and SCN/CoFe<sub>2</sub>O<sub>4</sub>/US with SCN/CoFe<sub>2</sub>O<sub>4</sub>/H<sub>2</sub>O<sub>2</sub>/US in Figure 8a, it is evident that the presence of both H<sub>2</sub>O<sub>2</sub> and ultrasonication greatly enhanced the removal efficiency by 3.5–4.1 times, i.e., the removal efficiencies increased from 11% to 45% in the former, and 27% to 96% in the latter. Additionally, by comparing the three catalysts, in the presence of H<sub>2</sub>O<sub>2</sub> and ultrasonication, SCN/CoFe<sub>2</sub>O<sub>4</sub> outperformed CoFe<sub>2</sub>O<sub>4</sub> and SCN by 2.2 and 6.8 times, respectively. Although a significant improvement was observed on the SCN/CoFe<sub>2</sub>O<sub>4</sub> nanocomposite by applying both H<sub>2</sub>O<sub>2</sub> and ultrasonication; by using H<sub>2</sub>O<sub>2</sub>/US as the benchmark, it was found that H<sub>2</sub>O<sub>2</sub> and ultrasonication had not brought much improvement but deterioration in the degradation efficiency for the catalysts CoFe<sub>2</sub>O<sub>4</sub> and SCN. This could be due to the non-optimum catalyst loading for each of these catalysts.

Figure 8b shows that the reactions follow pseudo-first-order kinetics. The *k* values obtained for the different systems are in the following order: SCN/CoFe<sub>2</sub>O<sub>4</sub>/H<sub>2</sub>O<sub>2</sub>/US (0.1369 min<sup>-1</sup>) > H<sub>2</sub>O<sub>2</sub>/US (0.0302 min<sup>-1</sup>) > CoFe<sub>2</sub>O<sub>4</sub>/H<sub>2</sub>O<sub>2</sub>/US (0.0283 min<sup>-1</sup>) > SCN/CoFe<sub>2</sub>O<sub>4</sub>/H<sub>2</sub>O<sub>2</sub> (0.0229 min<sup>-1</sup>) > SCN/CoFe<sub>2</sub>O<sub>4</sub> (0.02023 min<sup>-1</sup>) > SCN/CoFe<sub>2</sub>O<sub>4</sub>/US (0.0157 min<sup>-1</sup>) > SCN/H<sub>2</sub>O<sub>2</sub>/US (0.0058 min<sup>-1</sup>) > US alone (0.0067 min<sup>-1</sup>). Therefore, SCN/CoFe<sub>2</sub>O<sub>4</sub>/H<sub>2</sub>O<sub>2</sub>/US showed the highest synergistic effect than the other systems on the degradation of MB.

### 3.5. Effect of the Type of Organic Dye on Sonodegradation

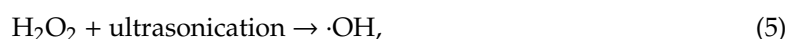
The capability of SCN/CoFe<sub>2</sub>O<sub>4</sub> nanocomposite in treating different types of organic dyes—RhB and CR—under the same conditions was evaluated, and the results are shown in Figure 9. The degradation efficiencies of RhB, CR and MB were 20%, 58%, and 83%, respectively. The significant difference can be attributed to the difference in dye sizes, structural compositions and electric charges [6–8]. Degradation of mixed organic dyes is therefore a challenging study worth investigating further.

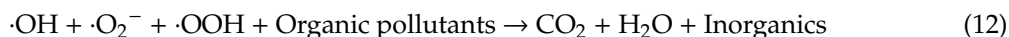


**Figure 9.** Effect of the type of organic dye on sonodegradation. Experimental conditions: [Dye concentration] = 25 ppm, [sonocatalyst] = 1 g/L, [H<sub>2</sub>O<sub>2</sub>] = 4 vol %.

### 3.6. Study of the Possible Mechanism of Sonodegradation

The enhancement of the sonodegradation can be through both chemical and physical processes [57]. The two major phenomena that originate from the ultrasonic-cavitation effect are ‘hot spots’ and sonoluminescence. The hot spots stimulate the sonolysis of H<sub>2</sub>O to produce ·OH and hydrogen radicals (·H) as shown in Equation (3). Sonoluminescence is generated when sound waves with sufficient intensity results in the formation of light [58]. Therefore, both SCN and CoFe<sub>2</sub>O<sub>4</sub> can be excited to produce sonogenerated e<sup>-</sup>-h<sup>+</sup> in the presence of visible light. It is known that the bandgap of CoFe<sub>2</sub>O<sub>4</sub> (1.37 eV) is lower than the SCN (2.47 eV), which causes the movement of electrons from SCN to CoFe<sub>2</sub>O<sub>4</sub> [59]. The electrons readily excite from the conduction band (CB) of SCN to the CB of CoFe<sub>2</sub>O<sub>4</sub>. Conversely, the sonogenerated holes in the valence band (VB) of CoFe<sub>2</sub>O<sub>4</sub> also get migrated to the VB of SCN. Hence, the reduction of the recombination rate due to the migration of sonogenerated electrons and holes in the opposite direction leads to the enhancement of sonocatalytic degradation. Further, the highly reactive ·OH is produced by the reaction of electrons in the CB with H<sub>2</sub>O<sub>2</sub>, which facilitate the degradation process [7]. The adsorbed OH<sup>-</sup> anions or H<sub>2</sub>O<sub>2</sub> onto the surface of the SCN react with the sonogenerated holes to form ·OH. Similarly, the interaction of adsorbed O<sub>2</sub> with the CB electrons generates ·O<sub>2</sub><sup>-</sup> and ·OOH, which aids in the indirect degradation of the organic dye solution. These active species oxidize the dye molecule into CO<sub>2</sub>, H<sub>2</sub>O, or NH<sub>4</sub><sup>+</sup> [8,60,61]. As is known, CoFe<sub>2</sub>O<sub>4</sub> possess more positive CB when compared with SCN. Hence, CoFe<sub>2</sub>O<sub>4</sub> in the SCN/CoFe<sub>2</sub>O<sub>4</sub> nanocomposite acts as a sink for generated electrons, whereas SCN acts as an acceptor for the promotion of interfacial electron transfer process. Equations (3) to (12) describe the chemical sonocatalytic process of SCN/CoFe<sub>2</sub>O<sub>4</sub> nanocomposite.





### 3.7. Reusability and Stability of SCN/CoFe<sub>2</sub>O<sub>4</sub> Nanocomposite

One of the important factors in the dye degradation process is the reusability of the catalysts. The practical usability and stability of the SCN/CoFe<sub>2</sub>O<sub>4</sub> nanocomposite under constant experimental conditions were investigated, and the results are shown in Figure 10a. After the sonodegradation experiment, the catalyst collected was washed with ethanol/water and dried at 60 °C for the subsequent runs. The degradation efficiencies were found to be 98%, 97%, 95%, 95%, 93%, and 91% for five successive cycles, with concentration measurement errors of 15%. Further, the structural stability of the recovered sample was studied by XRD as shown in Figure 10b. It is confirmed from the result that insignificant changes were observed after the third cycle of reusability.

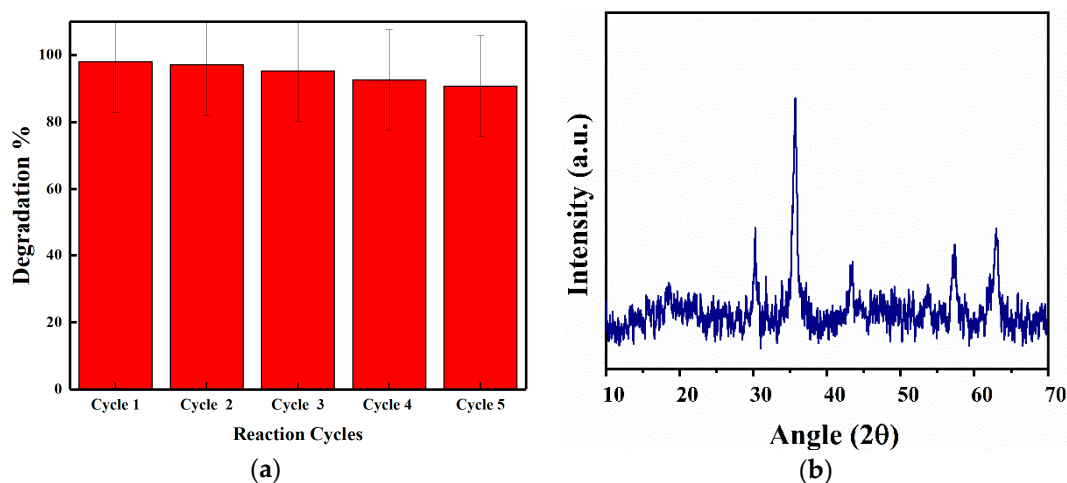


**Figure 10.** (a) Recyclability of SCN/CoFe<sub>2</sub>O<sub>4</sub> nanocomposite; (b) FT-IR of recovered SCN/CoFe<sub>2</sub>O<sub>4</sub> nanocomposite after the third cycle.

## 4. Conclusions

The SCN/CoFe<sub>2</sub>O<sub>4</sub> nanocomposite was successfully synthesized using ultrasonication method. The nanocomposite was composed of aggregated nanoparticles of CoFe<sub>2</sub>O<sub>4</sub> on a sheet-like SCN structure. Its bandgap energy was estimated to be 1.85 eV. XPS confirmed the presence of C, Co, Fe, O, N, and S elements in the atomic ratios of 54.39%, 2.03%, 39.83%, 2.36%, and 0.94%, respectively. The effects of the important experimental parameters such as catalyst dosage and H<sub>2</sub>O<sub>2</sub> loading on the MB degradation were analyzed. For the degradation of 25-ppm methylene blue, the best operating condition was found to be at a catalyst dosage of 1 g/L and 4 vol % of H<sub>2</sub>O<sub>2</sub> loading. In the presence of 4 vol % H<sub>2</sub>O<sub>2</sub>, the SCN/CoFe<sub>2</sub>O<sub>4</sub> nanocomposite demonstrated a high degradation efficiency of 96% within a reaction time of 20 min in the sonocatalytic degradation of 25-ppm methylene blue, in comparison with SCN (14%) and CoFe<sub>2</sub>O<sub>4</sub> (43%). It was also found that both ultrasonication and H<sub>2</sub>O<sub>2</sub> improved the methylene-blue degradation efficiency of SCN/CoFe<sub>2</sub>O<sub>4</sub> by 3.5–4.1 times. The sonocatalysis efficiencies for methylene blue, Congo-red, and rhodamine B were found to be 83%, 58%, and 20%, respectively. Further, the reusability test of SCN/CoFe<sub>2</sub>O<sub>4</sub> sonocatalyst revealed insignificant deterioration after the fifth cycle. In summary, the present work can inspire a low-cost, green sonocatalyst for the degradation of organic wastewater pollutants.

**Author Contributions:** Conceptualization and writing—original draft preparation, S.K.; validation and formal analysis, G.-T.P.; writing—review and editing, S.C.; supervision and funding acquisition, T.C.-K.Y. All authors have read and agreed to the published version of the manuscript.

**Funding:** This research received no external funding.

**Acknowledgments:** We thank the Precision Analysis and Materials Research Centre, National Taipei University of Technology, Taipei, Taiwan, for providing all the analytical facilities to this research. The authors also thank Faizan Husain for his helpful comments.

**Conflicts of Interest:** The authors declare no conflict of interest.

## References

1. Guo, S.; Tang, Y.; Xie, Y.; Tian, C.; Feng, Q.; Zhou, W.; Jiang, B. P-doped tubular g-C<sub>3</sub>N<sub>4</sub> with surface carbon defects: Universal synthesis and enhanced visible-light photocatalytic hydrogen production. *Appl. Catal. B Environ.* **2017**, *218*, 664–671. [[CrossRef](#)]
2. Liu, Y.; Li, M.; Zhang, Q.; Qin, P.; Wang, X.; He, G.; Li, L. One-step synthesis of WO<sub>3</sub>-CuS nanosheets heterojunction with enhanced photocatalytic performance for methylene blue degradation and Cr (VI) reduction. *J. Chem. Technol. Biotechnol.* **2019**. [[CrossRef](#)]
3. Konstantinou, I.K.; Albanis, T.A. TiO<sub>2</sub>-assisted photocatalytic degradation of azo dyes in aqueous solution: Kinetic and mechanistic investigations: A review. *Appl. Catal. B Environ.* **2004**, *49*, 1–14. [[CrossRef](#)]
4. Akpan, U.G.; Hameed, B.H. Parameters affecting the photocatalytic degradation of dyes using TiO<sub>2</sub>-based photocatalysts: A review. *J. Hazard. Mater.* **2009**, *170*, 520–529. [[CrossRef](#)]
5. Zhang, J.; Zhou, Y.; Jiang, M.; Li, J.; Sheng, J. Removal of methylene blue from aqueous solution by adsorption on pyrophyllite. *J. Mol. Liq.* **2015**, *209*, 267–271. [[CrossRef](#)]
6. Ertugay, N.; Acar, F.N. The degradation of Direct Blue 71 by sono, photo and sonophotocatalytic oxidation in the presence of ZnO nanocatalyst. *Appl. Surf. Sci.* **2014**, *318*, 121–126. [[CrossRef](#)]
7. Hassani, A.; Eghbali, P.; Metin, Ö. Sonocatalytic removal of methylene blue from water solution by cobalt ferrite/mesoporous graphitic carbon nitride (CoFe<sub>2</sub>O<sub>4</sub>/mpg-C<sub>3</sub>N<sub>4</sub>) nanocomposites: Response surface methodology approach. *Environ. Sci. Pollut. Res.* **2018**, *25*, 32140–32155. [[CrossRef](#)]
8. Hassani, A.; Çelikdağ, G.; Eghbali, P.; Sevim, M.; Karaca, S.; Metin, Ö. Heterogeneous sono-Fenton-like process using magnetic cobalt ferrite-reduced graphene oxide (CoFe<sub>2</sub>O<sub>4</sub>-rGO) nanocomposite for the removal of organic dyes from aqueous solution. *Ultrason. Sonochem.* **2018**, *40*, 841–852. [[CrossRef](#)]
9. Sadhanala, H.K.; Maddegalla, A.; Nanda, K. Thioacetamide-derived nitrogen and sulfur co-doped carbon nanoparticles used for label-free detection of copper (ii) ions and bioimaging applications. *New J. Chem.* **2017**, *41*, 13742–13746. [[CrossRef](#)]
10. Hu, S.; Yang, L.; Tian, Y.; Wei, X.; Ding, J.; Zhong, J.; Chu, P.K. Non-covalent doping of graphitic carbon nitride with ultrathin graphene oxide and molybdenum disulfide nanosheets: An effective binary heterojunction photocatalyst under visible light irradiation. *J. Colloid Interface Sci.* **2014**, *431*, 42–49. [[CrossRef](#)]
11. Kumar, A.; Yadav, R.K.; Park, N.-J.; Baeg, J.-O. Facile one-pot two-step synthesis of novel in situ selenium-doped carbon nitride nanosheet photocatalysts for highly enhanced solar fuel production from CO<sub>2</sub>. *ACS Appl. Nano Mater.* **2017**, *1*, 47–54. [[CrossRef](#)]
12. Feng, S.; Yan, P.; Xu, L.; Xia, J.; Li, H. Exploitation of a photoelectrochemical sensing platform for bisphenol A quantitative determination using Cu/graphitic carbon nitride nanocomposites. *Chin. Chem. Lett.* **2018**, *29*, 1629–1632. [[CrossRef](#)]
13. Rivera-Tapia, E.D.; Fajardo, C.A.; Ávila-Vega, Á.J.; Ávila, C.F.; Sánchez-Arévalo, F.M.; Chango-Villacís, I.; Quiroz-Chávez, F.J.; Santoyo-Salazar, J.; Dante, R.C. Synthesis of boron carbon nitride oxide (BCNO) from urea and boric acid. *Fuller. Nanotub. Carbon Nanostruct.* **2016**, *24*, 8–12. [[CrossRef](#)]
14. Kong, W.; Zhang, X.; Chang, B.; Zhou, Y.; Zhang, S.; He, G.; Yang, B.; Li, J. Fabrication of B doped g-C<sub>3</sub>N<sub>4</sub>/TiO<sub>2</sub> heterojunction for efficient photoelectrochemical water oxidation. *Electrochim. Acta* **2018**, *282*, 767–774. [[CrossRef](#)]
15. Zhou, Y.; Lv, W.; Zhu, B.; Tong, F.; Pan, J.; Bai, J.; Zhou, Q.; Qin, H. Template-Free One-Step Synthesis of g-C<sub>3</sub>N<sub>4</sub> Nanosheets with Simultaneous Porous Network and S-Doping for Remarkable Visible-Light-Driven Hydrogen Evolution. *ACS Sustain. Chem. Eng.* **2019**, *7*, 5801–5807. [[CrossRef](#)]

16. Liu, Z.; Jiang, Y.; Liu, X.; Zeng, G.; Shao, B.; Liu, Y.; Liu, Y.; Zhang, W.; Yan, M.; He, X. Silver chromate modified sulfur doped graphitic carbon nitride microrod composites with enhanced visible-light photoactivity towards organic pollutants degradation. *Compos. Part B Eng.* **2019**, *173*, 106918. [[CrossRef](#)]
17. Cao, S.; Huang, Q.; Zhu, B.; Yu, J. Trace-level phosphorus and sodium co-doping of g-C<sub>3</sub>N<sub>4</sub> for enhanced photocatalytic H<sub>2</sub> production. *J. Power Sources* **2017**, *351*, 151–159. [[CrossRef](#)]
18. Liu, B.; Ye, L.; Wang, R.; Yang, J.; Zhang, Y.; Guan, R.; Tian, L.; Chen, X. Phosphorus-doped graphitic carbon nitride nanotubes with amino-rich surface for efficient CO<sub>2</sub> capture, enhanced photocatalytic activity, and product selectivity. *ACS Appl. Mater. Interfaces* **2018**, *10*, 4001–4009. [[CrossRef](#)]
19. Kumar, P.; Boukherroub, R.; Shankar, K. Sunlight-driven water-splitting using two-dimensional carbon based semiconductors. *J. Mater. Chem. A* **2018**, *6*, 12876–12931. [[CrossRef](#)]
20. Nasir, M.S.; Yang, G.; Ayub, I.; Wang, S.; Wang, L.; Wang, X.; Yan, W.; Peng, S.; Ramakarishna, S. Recent development in graphitic carbon nitride based photocatalysis for hydrogen generation. *Appl. Catal. B Environ.* **2019**, 117855. [[CrossRef](#)]
21. Zhou, L.; Zhang, H.; Sun, H.; Liu, S.; Tade, M.O.; Wang, S.; Jin, W. Recent advances in non-metal modification of graphitic carbon nitride for photocatalysis: A historic review. *Catal. Sci. Technol.* **2016**, *6*, 7002–7023. [[CrossRef](#)]
22. Zhang, Y.; Zong, S.; Cheng, C.; Shi, J.; Guan, X.; Lu, Y.; Guo, L. One-pot annealing preparation of Na-doped graphitic carbon nitride from melamine and organometallic sodium salt for enhanced photocatalytic H<sub>2</sub> evolution. *Int. J. Hydrog. Energy* **2018**, *43*, 13953–13961. [[CrossRef](#)]
23. Jiang, L.; Yuan, X.; Pan, Y.; Liang, J.; Zeng, G.; Wu, Z.; Wang, H. Doping of graphitic carbon nitride for photocatalysis: A review. *Appl. Catal. B Environ.* **2017**, *217*, 388–406. [[CrossRef](#)]
24. Shcherban, N.D.; Filonenko, S.M.; Ovcharov, M.L.; Mishura, A.M.; Skoryk, M.A.; Aho, A.; Murzin, D.Y. Simple method for preparing of sulfur-doped graphitic carbon nitride with superior activity in CO<sub>2</sub> photoreduction. *ChemistrySelect* **2016**, *1*, 4987–4993. [[CrossRef](#)]
25. Wen, J.; Xie, J.; Chen, X.; Li, X. A review on g-C<sub>3</sub>N<sub>4</sub>-based photocatalysts. *Appl. Surf. Sci.* **2017**, *391*, 72–123. [[CrossRef](#)]
26. Song, L.; Zhang, S.; Wu, X.; Wei, Q. A metal-free and graphitic carbon nitride sonocatalyst with high sonocatalytic activity for degradation methylene blue. *Chem. Eng. J.* **2012**, *184*, 256–260. [[CrossRef](#)]
27. Dong, G.; Zhang, Y.; Pan, Q.; Qiu, J. A fantastic graphitic carbon nitride (g-C<sub>3</sub>N<sub>4</sub>) material: Electronic structure, photocatalytic and photoelectronic properties. *J. Photochem. Photobiol. C Photochem. Rev.* **2014**, *20*, 33–50. [[CrossRef](#)]
28. Abazari, R.; Mahjoub, A.R.; Sanati, S.; Rezvani, Z.; Hou, Z.; Dai, H. Ni–Ti layered double hydroxide@graphitic carbon nitride nanosheet: A novel nanocomposite with high and ultrafast sonophotocatalytic performance for degradation of antibiotics. *Inorg. Chem.* **2019**, *58*, 1834–1849. [[CrossRef](#)]
29. Kong, J.; Lai, X.; Rui, Z.; Ji, H.; Ji, S. Multichannel charge separation promoted ZnO/P25 heterojunctions for the photocatalytic oxidation of toluene. *Chin. J. Catal.* **2016**, *37*, 869–877. [[CrossRef](#)]
30. Nirumand, L.; Farhadi, S.; Zabardasti, A.; Khataee, A. Copper ferrite nanoparticles supported on MIL-101/reduced graphene oxide as an efficient and recyclable sonocatalyst. *J. Taiwan Inst. Chem. Eng.* **2018**, *93*, 674–685. [[CrossRef](#)]
31. Ghobadifard, M.; Farhadi, S.; Mohebbi, S. Sonocatalytic performance of magnetic flower-like CoFe<sub>2</sub>O<sub>4</sub> nanoparticles prepared from a heterometallic oxo-centered trinuclear complex under microwave irradiation. *Polyhedron* **2018**, *155*, 66–76. [[CrossRef](#)]
32. López, Y.O.; Vázquez, H.M.; Gutiérrez, J.S.; Velderrain, V.G.; Ortiz, A.L.; Martínez, V.C. Synthesis method effect of CoFe<sub>2</sub>O<sub>4</sub> on its photocatalytic properties for H<sub>2</sub> production from water and visible light. *J. Nanomater.* **2015**, *16*, 76.
33. Safari, J.; Zarnegar, Z. Brønsted acidic ionic liquid based magnetic nanoparticles: A new promoter for the Biginelli synthesis of 3,4-dihydropyrimidin-2(1H)-ones/thiones. *New J. Chem.* **2014**, *38*, 358–365. [[CrossRef](#)]
34. Nivetha, R.; Chella, S.; Kollu, P.; Jeong, S.K.; Bhatnagar, A.; Andrews, N.G. Cobalt and nickel ferrites based graphene nanocomposites for electrochemical hydrogen evolution. *J. Magn. Magn. Mater.* **2018**, *448*, 165–171. [[CrossRef](#)]
35. Shao, Z.; Zeng, T.; He, Y.; Zhang, D.; Pu, X. A novel magnetically separable CoFe<sub>2</sub>O<sub>4</sub>/Cd<sub>0.9</sub>Zn<sub>0.1</sub>S photocatalyst with remarkably enhanced H<sub>2</sub> evolution activity under visible light irradiation. *Chem. Eng. J.* **2019**, *359*, 485–495. [[CrossRef](#)]

36. Chen, J.; Zhao, D.; Diao, Z.; Wang, M.; Shen, S. Ferrites boosting photocatalytic hydrogen evolution over graphitic carbon nitride: A case study of (Co, Ni)Fe<sub>2</sub>O<sub>4</sub> modification. *Sci. Bull.* **2016**, *61*, 292–301. [[CrossRef](#)]
37. Zhong, M.; Fei, P.; Fu, X.; Lei, Z.; Su, B. Synthesis of PS–CoFe<sub>2</sub>O<sub>4</sub> composite nanomaterial with improved magnetic properties by a one-step solvothermal method. *Ind. Eng. Chem. Res.* **2013**, *52*, 8230–8235. [[CrossRef](#)]
38. Thomas, B.; Alexander, L. Enhanced synergetic effect of Cr (VI) ion removal and anionic dye degradation with superparamagnetic cobalt ferrite meso–macroporous nanospheres. *Appl. Nanosci.* **2018**, *8*, 125–135. [[CrossRef](#)]
39. Liu, Z.; Xu, G.; Zhang, M.; Xiong, K.; Meng, P. Synthesis of CoFe<sub>2</sub>O<sub>4</sub>/RGO nanocomposites by click chemistry and electromagnetic wave absorption properties. *J. Mater. Sci. Mater. Electron.* **2016**, *27*, 9278–9285. [[CrossRef](#)]
40. Qin, H.; Lv, W.; Bai, J.; Zhou, Y.; Wen, Y.; He, Q.; Tang, J.; Wang, L.; Zhou, Q. Sulfur-doped porous graphitic carbon nitride heterojunction hybrids for enhanced photocatalytic H<sub>2</sub> evolution. *J. Mater. Sci.* **2019**, *54*, 4811–4820. [[CrossRef](#)]
41. Joseph, S.; Abraham, S.; Priyanka, R.N.; Abraham, T.; Suresh, A.; Mathew, B. In situ S-doped ultrathin gC<sub>3</sub>N<sub>4</sub> nanosheets coupled with mixed-dimensional (3D/1D) nanostructures of silver vanadates for enhanced photocatalytic degradation of organic pollutants. *New J. Chem.* **2019**, *43*, 10618–10630. [[CrossRef](#)]
42. Ge, L.; Han, C.; Xiao, X.; Guo, L.; Li, Y. Enhanced visible light photocatalytic hydrogen evolution of sulfur-doped polymeric g-C<sub>3</sub>N<sub>4</sub> photocatalysts. *Mater. Res. Bull.* **2013**, *48*, 3919–3925. [[CrossRef](#)]
43. Kargar, A.; Yavuz, S.; Kim, T.K.; Liu, C.-H.; Kuru, C.; Rustomji, C.S.; Jin, S.; Bandaru, P.R. Solution-processed CoFe<sub>2</sub>O<sub>4</sub> nanoparticles on 3D carbon fiber papers for durable oxygen evolution reaction. *ACS Appl. Mater. Interfaces* **2015**, *7*, 17851–17856. [[CrossRef](#)] [[PubMed](#)]
44. Chang, C.-J.; Lee, Z.; Chu, K.-W.; Wei, Y.-H. CoFe<sub>2</sub>O<sub>4</sub>@ZnS core–shell spheres as magnetically recyclable photocatalysts for hydrogen production. *J. Taiwan Inst. Chem. Eng.* **2016**, *66*, 386–393. [[CrossRef](#)]
45. Ke, L.; Li, P.; Wu, X.; Jiang, S.; Luo, M.; Liu, Y.; Le, Z.; Sun, C.; Song, S. Graphene-like sulfur-doped g-C<sub>3</sub>N<sub>4</sub> for photocatalytic reduction elimination of UO<sub>2</sub><sup>2+</sup> under visible Light. *Appl. Catal. B Environ.* **2017**, *205*, 319–326. [[CrossRef](#)]
46. Shi, C.; Chen, M.; Han, X.; Bi, Y.; Huang, L.; Zhou, K.; Zheng, Z. Thiacalix[4]arene-supported tetradecanuclear cobalt nanocage cluster as precursor to synthesize CoO/Co<sub>9</sub>S<sub>8</sub>@CN composite for supercapacitor application. *Inorg. Chem. Front.* **2018**, *5*, 1329–1335. [[CrossRef](#)]
47. Sadiq, M.M.J.; Shenoy, U.S.; Bhat, D.K. Synthesis of BaWO<sub>4</sub>/NRGO–gC<sub>3</sub>N<sub>4</sub> nanocomposites with excellent multifunctional catalytic performance via microwave approach. *Front. Mater. Sci.* **2018**, *12*, 247–263. [[CrossRef](#)]
48. Cao, S.; Fan, B.; Feng, Y.; Chen, H.; Jiang, F.; Wang, X. Sulfur-doped g-C<sub>3</sub>N<sub>4</sub> nanosheets with carbon vacancies: General synthesis and improved activity for simulated solar-light photocatalytic nitrogen fixation. *Chem. Eng. J.* **2018**, *353*, 147–156. [[CrossRef](#)]
49. Chang, Q.; Yang, S.; Li, L.; Xue, C.; Li, Y.; Wang, Y.; Hu, S.; Yang, J.; Zhang, F. Loading sulfur and nitrogen co-doped carbon dots onto gC<sub>3</sub>N<sub>4</sub> nanosheets for an efficient photocatalytic reduction of 4-nitrophenol. *Dalton Trans.* **2018**, *47*, 6435–6443. [[CrossRef](#)]
50. Xiong, P.; Chen, Q.; He, M.; Sun, X.; Wang, X. Cobalt ferrite–polyaniline heteroarchitecture: A magnetically recyclable photocatalyst with highly enhanced performances. *J. Mater. Chem.* **2012**, *22*, 17485–17493. [[CrossRef](#)]
51. Sun, X.; Gao, L.; Guo, C.; Zhang, Y.; Kuang, X.; Yan, T.; Ji, L.; Wei, Q. Sulfur incorporated CoFe<sub>2</sub>O<sub>4</sub>/multiwalled carbon nanotubes toward enhanced oxygen evolution reaction. *Electrochim. Acta* **2017**, *247*, 843–850. [[CrossRef](#)]
52. Navarro-Pardo, F.; Tong, X.; Selopal, G.S.; Cloutier, S.G.; Sun, S.; Tavares, A.C.; Zhao, H.; Wang, Z.M.; Rosei, F. Graphene oxide/cobalt-based nanohybrid electrodes for robust hydrogen generation. *Appl. Catal. B Environ.* **2019**, *245*, 167–176. [[CrossRef](#)]
53. Rodríguez-Rodríguez, A.A.; Moreno-Trejo, M.B.; Meléndez-Zaragoza, M.J.; Collins-Martínez, V.; López-Ortiz, A.; Martínez-Guerra, E.; Sánchez-Domínguez, M. Spinel-type ferrite nanoparticles: Synthesis by the oil-in-water microemulsion reaction method and photocatalytic water-splitting evaluation. *Int. J. Hydrog. Energy* **2019**, *44*, 12421–12429. [[CrossRef](#)]

54. Zhang, Z.; Li, W.; Zou, R.; Kang, W.; San Chui, Y.; Yuen, M.F.; Lee, C.-S.; Zhang, W. Layer-stacked cobalt ferrite (CoFe<sub>2</sub>O<sub>4</sub>) mesoporous platelets for high-performance lithium ion battery anodes. *J. Mater. Chem. A* **2015**, *3*, 6990–6997. [[CrossRef](#)]
55. de Lima Alves, T.M.; Amorim, B.F.; Torres, M.A.M.; Bezerra, C.G.; de Medeiros, S.N.; Gastelois, P.L.; Outon, L.E.F.; de Almeida Macedo, W.A. Wasp-waisted behavior in magnetic hysteresis curves of CoFe<sub>2</sub>O<sub>4</sub> nanopowder at a low temperature: Experimental evidence and theoretical approach. *RSC Adv.* **2017**, *7*, 22187–22196. [[CrossRef](#)]
56. Zhou, B.; Lee, L.-K. Catalyst and Process for Direct Catalytic Production of Hydrogen Peroxide, (H<sub>2</sub>O<sub>2</sub>). U.S. Patent 6,168,775, 2 January 2001.
57. Lee, G.; Chu, K.H.; Al-Hamadani, Y.A.; Park, C.M.; Jang, M.; Heo, J.; Her, N.; Kim, D.-H.; Yoon, Y. Fabrication of graphene-oxide/ $\beta$ -Bi<sub>2</sub>O<sub>3</sub>/TiO<sub>2</sub>/Bi<sub>2</sub>Ti<sub>2</sub>O<sub>7</sub> heterojuncted nanocomposite and its sonocatalytic degradation for selected pharmaceuticals. *Chemosphere* **2018**, *212*, 723–733. [[CrossRef](#)]
58. Siadatnasab, F.; Farhadi, S.; Khataee, A. Sonocatalytic performance of magnetically separable CuS/CoFe<sub>2</sub>O<sub>4</sub> nanohybrid for efficient degradation of organic dyes. *Ultrason. Sonochem.* **2018**, *44*, 359–367. [[CrossRef](#)]
59. Borgohain, C.; Senapati, K.K.; Sarma, K.; Phukan, P. A facile synthesis of nanocrystalline CoFe<sub>2</sub>O<sub>4</sub> embedded one-dimensional ZnO hetero-structure and its use in photocatalysis. *J. Mol. Catal. A Chem.* **2012**, *363*, 495–500. [[CrossRef](#)]
60. Huang, F.; Chen, L.; Wang, H.; Yan, Z. Analysis of the degradation mechanism of methylene blue by atmospheric pressure dielectric barrier discharge plasma. *Chem. Eng. J.* **2010**, *162*, 250–256. [[CrossRef](#)]
61. Sajjadi, S.; Khataee, A.; Kamali, M. Sonocatalytic degradation of methylene blue by a novel graphene quantum dots anchored CdSe nanocatalyst. *Ultrason. Sonochem.* **2017**, *39*, 676–685. [[CrossRef](#)]



© 2020 by the authors. Licensee MDPI, Basel, Switzerland. This article is an open access article distributed under the terms and conditions of the Creative Commons Attribution (CC BY) license (<http://creativecommons.org/licenses/by/4.0/>).